XX IMEKO World Congress
Metrology for Green Growth
September 9–14, 2012, Busan, Republic of Korea.

LASER SPECKLE SIMULATION ON A ROUGH WETTING PROBLEM

D. Hofer, and B.G. Zagar

Institute for Measurement Technology, Johannes Kepler University, Linz, Austria,
dominik.hofer@jku.at

Abstract — Computing numerical approximations of the Huygens-Fresnel principle in three dimensions is a rather time (and hardware) demanding task, but thanks to massive parallelization in GPGPU enabled graphics cards these computations can be sped up considerably. A newly developed software framework is capable to simulate a large portion of wave propagation related problems. It seems suited to generate laser speckle images for various real physical setups which were used to measure the surface roughness of sheet metal or the oil film thickness on top of it. This paper gives a short survey on rough wetting theory, it introduces the core parts of the software, and finally it shows some test cases using apertures and their known Fraunhofer diffraction patterns.

Keywords — laser speckle simulation framework, GPGPU, GPUmat, surface roughness, rough wetting

1. INTRODUCTION & MOTIVATION

Corrosion of iron and its alloys, commonly termed 'rust', can be a severe problem in automotive sheet metal production. In finished products the metal is usually coated by varnish or any other protective coating. Prior to this finishing the metal is often protected by a thin film of oil. The very thickness of this film is of concern for any manufacturer of sheet steel. It must maintain a minimum thickness to fulfill its protective purpose but it should not exceed a maximum thickness because it could affect subsequent processes and produce unnecessary costs.

Numerous methods to determine the layer thickness of fluids on smooth surfaces are known. To name a few examples some techniques employ changes in capacitance [1], Raman backscattering [2], the temperature gradient [3] or ultrasound [4]. However, if the surface is rough and the film thickness is in the range of the roughness the film fills in the pits and grooves of the surface so that adhesive forces between the materials and cohesive forces within the film reach an equilibrium. The film thickness varies rapidly over distance, thus integral effects like the change of capacitance or principles based on long wavelength radiation yield unreliable results due to their rather low spatial resolutions.

Rough wetting seems to be a clue, since Andelman et al. [5, 6] established a connection between the profile of the surface/fluid interface of an oil covered rough plane and the profile of the fluid/air interface atop. It was found out that the liquid acts as a low-pass to the underlying surface roughness, i. e. the wet surface seems to get smoother with increasing thickness of the film and roughness measurements can provide information on the film thickness.

Preceding evaluations by Lettner et al. [7] focused on laser speckle techniques [8, 9] to measure surface roughness, and thus oil film thickness, locally. Various measurement setups were devised and tested thoroughly, but the adjustment and evaluation of the different devices proved to be tedious. Within short time the wish to simulate the respective outcomes lead to the development of the custom software toolbox presented throughout this paper.

Numerical laser speckle simulations, like the ones given by Goodman [10] or Equis and Jacquot [11], often use relations in the Fourier domain which make inherent use of the Huygens-Fresnel principle under a paraxial approximation. Diffuse reflections of laser light on any rough surface do not satisfy this assumption. That is why the core part of this contribution employs a numerical approximation of the Huygens-Fresnel principle in the spatial domain. It involves a sum over all elements of an electro-

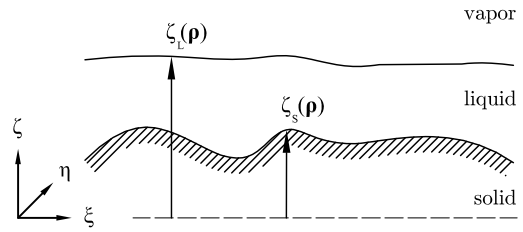

Fig. 1: A liquid film between a vapor and a rough solid surface. The solid/liquid and liquid/vapor interfaces are at heights $\zeta_S(\rho)$ and $\zeta_L(\rho)$ above the $\{\xi, \eta, 0\}$ reference plane [5].

magnetic field within an aperture plane to compute the field in a single arbitrary location in another plane of interest. Only mild approximations, a discretization of both electromagnetic fields and the use of finite precision arithmetics [12] affect the computation result.

Laser speckle related simulations require high spatial resolutions in the order of the used wavelength, e. g. 550 nm for green light, which yield rather large matrix sizes when using realistic dimensions for the setup. Computations on a sequentially working CPU proved to be unfeasible due to the long computation time needed to solve even simple problems, e. g. we estimated a week to solve the wave propagation from a 2000×2000 points source aperture to a 512×512 points destination field. Fortunately, the freeware software toolbox 'GPUmat' for Mathworks' MATLAB provides a convenient way to access the general purpose computation capabilities on the graphics processing units of NVIDIA CUDA™ enabled graphics cards. It speeds up computing, depending on the respective problem size, by at least a factor of 30 to 50. The GPU accelerated solver finished above example problem in approximately six hours, 36 times faster than the same algorithm running on an Intel® Core™2 Q9550 2.83 GHz.

This papers subsequent sections are concerned with the physical models and principles which were used to simulate the wave propagation of monochromatic light, the validation of the simulation results and a short conclusion. Finally, an acknowledgement and references conclude the paper.

2. ROUGH SURFACES

In this section a short introduction to the theory of rough wetting is followed by an algorithm to define an artificial surface.

A Rough Wetting

Complete wetting with zero contact angle describes a thin layer of liquid completely covering a solid surface [13, 14] as shown in Fig. 1. The solid surface $\zeta_S(\rho)$ is specified for each vector $\rho = \{\xi, \eta\}$ in a two-dimensional reference plane [5]. Andelman et al. determined the liquid/vapor interface $\zeta_L(\rho)$ above the solid surface by minimizing the free energy $\mathbf{F}$ which is built up of solid/vapor, solid/liquid and liquid/vapor surface tensions, molecular interactions between the solid and the liquid surfaces and the chemical potential of the film. Linearization of the resulting integro-differential equation yields

$$\tilde{\zeta_L}(\mathbf{q}) = \tilde{\zeta_S}(\mathbf{q})\tilde{K}(\mathbf{q}) \,/\, \left(1 + \mathbf{q}^2\xi^2\right) \qquad (1)$$

where $\mathbf{q}$ is a frequency in periods/m, $\tilde{\zeta_L}(\mathbf{q})$, $\tilde{\zeta_S}(\mathbf{q})$ and $\tilde{K}(\mathbf{q})$ are the Fourier transforms of the liquid/vapor interface, the solid/liquid interface and a convolution kernel $K(\mathbf{q})$. ξ is the surface tension dependent *healing length*, whereas $K(\mathbf{q})$ contains energy related terms. Equation 1 acts as a low-pass filter on $\tilde{\zeta_S}(\mathbf{q})$, i. e. fast varying undulations of the metal surface are damped and the liquid surface gets smoother with increasing film thickness.

B An Artificial Surface

As a consequence for the proposed simulation model a surface $\zeta_{\mathrm{S,\ art}}(\rho)$ has to be generated. It is defined in a two step process, where at first an artificial Fourier transform $\tilde{\zeta}_{\mathrm{S0}}(\mathbf{q})$ of the surface determines most of its spectral properties and a subsequent scaling in the spatial domain guarantees a desired surface roughness. The spectrum for all frequencies $\mathbf{q}$ is given by

$$\left|\tilde{\zeta}_{\mathrm{S0}}(\mathbf{q})\right| = a(\mathbf{q}), \qquad (2)$$

$$\angle\left(\tilde{\zeta}_{\mathrm{S0}}(\mathbf{q})\right) = \mathcal{U}(-\pi, \pi), \qquad (3)$$

$$\tilde{\zeta}_{\mathrm{S0}}(\mathbf{q}) = \tilde{\zeta}^*_{\mathrm{S0}}(-\mathbf{q}).\,, \qquad (4)$$

where $a(\mathbf{q}) : \mathbb{R}^2 \to \mathbb{R}$ in Eqn. 2 may be an arbitrary function, e. g. a low-pass, which acts only on the magnitude of $\tilde{\zeta}_{\mathrm{S,\ art}}(\mathbf{q})$. The complex phase of each component of the spectrum is distributed uniformly on the unit circle by Eqn. 3 and finally the symmetry relation in Eqn. 4 guarantees $\zeta_{\mathrm{S0}}(\rho) \in \mathbb{R}$.

In the simplest case the function $a(\mathbf{q})$ may be a rotationally symmetric Gaussian low-pass [15]

$$a(\mathbf{q}) = \exp\left(-\left|\mathbf{q}\right| / (2\sigma^2)\right), \qquad (5)$$

where σ is the standard deviation of the Gaussian curve. A more sophisticated approach is to

make the function dependent on the direction of the vector $\mathbf{q} = \{q_1, q_2\}$ to simulate different spectral distributions along the spatial dimensions q_i by using different standard deviations $\{\sigma_1, \sigma_2\}$:

$$a(\mathbf{q}) = \exp\left(-\left(q_1/\sigma_1\right)^2 - \left(q_2/\sigma_2\right)^2 + 1\right).$$

The function evaluates to equal values on ellipses around the origin. This way grooves and rills can be simulated, albeit the parameters for real surfaces have to be determined by spatially resolved roughness measurements [16, 17].

Above formulae determine the relative magnitudes $|\tilde{\zeta}_{\mathrm{S0}}(\mathbf{q})|$ of the spectrum and give a rather arbitrary surface roughness $\zeta_{\mathrm{S0}}(\rho)$ in the spatial domain. In order to conclude the artificial surface generation a linear scaling by its absolute mean surface roughness $1/R_a$ and the desired roughness $R_{\mathrm{a,\,des}}$ has to be performed:

$$\zeta_{\mathrm{S,\,art}}(\rho) = \zeta_{\mathrm{S0}}(\rho) \cdot \frac{R_{\mathrm{a,\,des}}}{R_a}, \qquad (6)$$

with the mean surface roughness

$$R_a = \frac{1}{NM} \sum_{i=1}^{N} \sum_{j=1}^{M} |\zeta_{ij}|\,, \qquad \zeta_{ij} \in \zeta_{\mathrm{S0}}(\rho), \quad (7)$$

where N and M are the number of sampled points ζ_{ij} along the ξ- and η-directions of $\zeta_{\mathrm{S0}}(\rho)$.

For the numerical simulation of the discretized problem proper spatial resolutions $\{\Delta\xi, \Delta\eta\}$ along the respective dimensions have to be chosen. The discrete Fourier transform of size $N \times M$ and frequency resolution $\Delta\mathbf{q} = \{1/(N\,\Delta\xi), 1/(M\,\Delta\eta)\}$ is defined according to Eqns. 2 to 4 and an appropriate low-pass filter function is applied. At this stage aliasing is of no concern, since no sampling operation was involved in construction of $\tilde{\zeta}_{\mathrm{S0}}(\mathbf{q})$ or $\zeta_{\mathrm{S,\,art}}(\rho)$. However, the surface might be interpolated at new coordinates in a later stage of the simulation where aliasing might occur.

To simulate rough wetting a 'master surface', which should approximate a measured specimen of a dry surface, is generated. Wet surfaces are simulated either by a linear scaling of the master's roughness or by further low-pass filtering. The latter also allows control over the spectral distribution.

3. LIGHT & LASERS

Now, equipped with a suitable rough surface it is to be illuminated by monochromatic light.

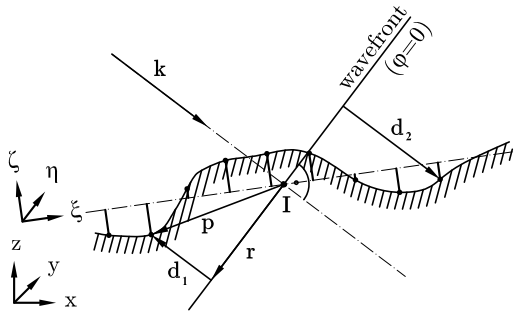

Fig. 2: Monochromatic light with a wave vector $\mathbf{k}$ is cast onto a rough surface. The distance $\mathbf{p}$ from the intersection point $\mathbf{I}$ of vector $\mathbf{k}$ and the reference surface $\zeta = 0$ is projected onto the wave vector and on the wavefront. This gives its propagation distance d and its beam radius r, respectively. d_1 depicts a negative and d_2 a positive phase term to add to the reference wavefront. $\{\xi, \eta, \zeta\}$ is the surface' coordinate system and $\{x, y, z\}$ is the global reference coordinate system.

A Illumination

The irradiance of monochromatic light in matter is given by

$$I(r) \approx \frac{cn\varepsilon_0}{2} \left|\underline{E}(r)\right|^2, \qquad (8)$$

where c is the speed of light in vacuum, n is the refractive index of the medium, ε_0 is the vacuum permittivity and $\underline{E}$ is the complex amplitude of the electric field. For a TEM_{00} mode laser beam of half-power diameter D the intensity $I(r)$ decreases with distance r to the principal axis of the laser and shows a Gaussian beam profile, but for $r \ll D$ the intensity can be assumed to be constant. The electric field oscillates unison on a plane wavefront, i. e. propagation by a distance d along the wave vector $\mathbf{k}$ equals a multiplication of the field by a phase term $\varphi = \exp(\imath k d)$, where $k = |\mathbf{k}|$ is the wave number.

Figure 2 depicts the basic principle to assign a complex electric field value to every point $\mathbf{p} = \{\xi, \eta, \zeta\}$ on a surface. In a first step the intersection of the laser axis with the surface reference plane is determined and the surface point is assigned a vector to this intersection point. Its projection onto the wavefront yields the radius r and onto the laser axis gives the distance d and thus the additional phase term to add.

The numerical approximation is straight forward, given a list of surface points, a wavelength and a function describing the electric field of the laser beam on a reference wavefront.

B Reflection & Polarization

Specular reflection is the mirror-like reflection of light on a surface, i. e. the angle of incidence between a light ray and the surface normal equals the angle of reflection between the surface normal and the reflected ray. In the simulation either the surface normal of the reference plane or local surface normals for every point can be used to calculate the direction of reflection in every point. While the former gives pure specular reflection for the whole surface, the latter results in diffuse reflection with an indicatrix dependent on the spatial derivatives $\{\frac{\partial\zeta}{\partial\xi}, \frac{\partial\zeta}{\partial\eta}\}$ of the surface. In software these are computed in every point of the grid by using finite differences from its next four neighbors. Their surface normals are computed by normalizing the cross product of these vectors.

Polarization effects are not yet implemented but would easily fit into the simulation framework. Necessary changes would be the use of a second electric field variable perpendicular to the first one, i. e. $\{\underline{E}_\xi, \underline{E}_\eta\}$ field components. Reflection or transmission on or into a medium with another refractive index alter both components according to the Fresnel equations [18]. Both fields are independent otherwise so that their combined observed intensity on a screen equals the superposition of their respective intensities. This addition to the software package renders the simulation of other optical components like polarizers or birefringent materials possible, albeit it doubles computation time and disk space requirements.

4. LIGHT PROPAGATION

The central task of the MATLAB toolbox is the computation of an image on a screen adjacent to a light reflecting surface or an illuminated aperture. This section covers the basic principle to calculate the electric field and the problems which come with its approximation.

A The Huygens-Fresnel principle

Light propagation and diffraction is appropriately described by the Huygens-Fresnel principle [19], which is shown in Fig. 3 for rectangular coordinates. It is given by

$$\underline{E}(x,y) = \frac{1}{\imath\lambda} \iint_\Sigma \underline{E}(\xi,\eta) \frac{\exp(\imath k r)}{r} \cos\theta \, ds, \quad (9)$$

where λ is the wavelength, $r = |\mathbf{r}|$ is a vector from an aperture to the a parallel screen, i. e. the distance z is constant, θ is the angle between $\mathbf{r}$ and the aperture surface normal $\mathbf{n}$ and $\underline{E}(x,y)$ and $\underline{E}(\xi,\eta)$ are the complex electric fields on the screen and the aperture Σ, respectively.

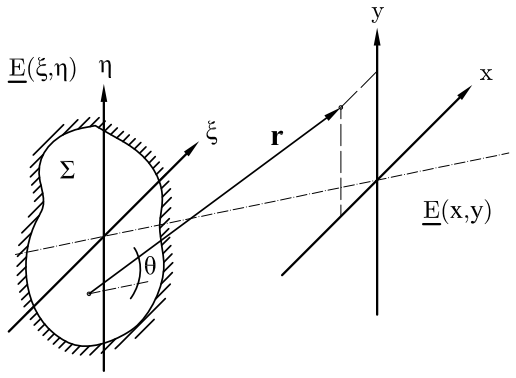

Fig. 3: A so-called 'phasor' or complex pointer of the electric field $\underline{E}(\xi,\eta)$ rotates by $k\,|\mathbf{r}|$ while propagating from the aperture Σ to the screen. The integral over contributions from all points in the aperture give the electric field $\underline{E}(x,y)$.

Only two approximations are made by using above principle. A scalar instead of a vector theory is used, but this is valid as long as the dimensions of the diffracting geometry are large in comparison to the wavelength λ. The second is the assumption that the observation distance is many wavelengths from the aperture, $r \gg \lambda$.

Note that the Huygens-Fresnel principle is only valid for plane apertures, so for rough surfaces an additional approximation is necessary to simulate diffraction. Fortunately $r \gg \zeta$ is true and a surface aperture can be approximated by using the full, three dimensional coordinates $\{\xi,\eta,\zeta\}$.

Projection on a rough surface is not an issue because one could use an infinite number of screens with different $z = z_0 \pm \zeta_{\max}$, where $\zeta_{\max}$ is the maximum amplitude of the surface roughness with respect to the mean value. Extracting only the electric field values at locations $\{x,y,z\}$ delivers the field on the rough aperture.

The discretization of Eqn. 9 is rather simple by replacing the integral with a sum over sampled values $\underline{E}(\xi_i,\eta_j)$ and ds with the area $\Delta\xi \times \Delta\eta$ of a grid cell on the source aperture. However, the operation has to be carried out for every point on the screen and thus is computational costly. As of today only MATLAB's vectorization methods and massive parallelization on the graphics card renders the problem solvable on a desktop computer in a reasonable time. In the current implementation 14 $N \times M$

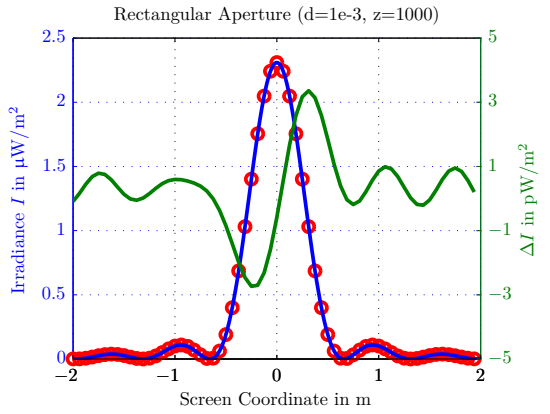

Fig. 4: The diffraction of a $1\,\mathrm{mm}^2$ quadratic aperture viewed at a screen which is located a 1000 m away. The simulation result in red color fits the theoretical Fraunhofer diffraction pattern in blue color exactly. Note that only 64 points of the approximation are plotted as dots to easily distinguish both curves. The difference between both approximations is plotted in green color, with its greatest magnitude estimated as $3.36\,\mathrm{pW/m}^2$.

sized arrays with double precision data and one complex data array for the electric field on the screen are stored in 1.5 GB GPU memory, holding up to 3000^2 values in each aperture array. Larger matrices can be split in partitions, computed separately and be finally superposed, due to the summing nature of the Huygens-Fresnel integral.

B Diffraction & Examples

A Fraunhofer diffraction pattern of a rectangular aperture was chosen to validate the results of the software framework. The intensity on a screen located at a distance z for an aperture with side lengths $\{2w_x, 2w_y\}$ and a monochromatic light source with wavelength λ is given by [10]

$$I(x,y) = A\,\mathrm{sinc}^2\left(\frac{2w_x x}{\lambda z}\right)\mathrm{sinc}^2\left(\frac{2w_y y}{\lambda z}\right), \tag{10}$$

with peak amplitude

$$A = \left(\frac{2w_x 2w_y}{\lambda z}\right)^2. \tag{11}$$

Figure 4 shows the simulation result which fits the theoretical prediction both in magnitude and locations of the minima and maxima.

Diffraction is also observed due to the partition of the aperture in discrete pixels. These form a grid structure which produces an additional diffraction pattern to the one of the finite

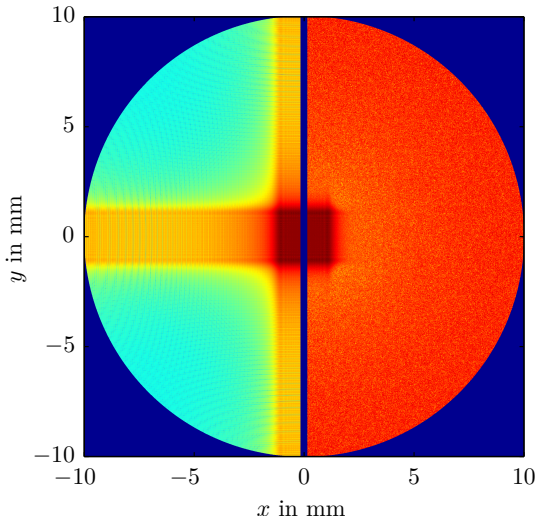

Fig. 5: Two half-images of simulation results for a 2.56×2.56 mm^2 rectangular aperture. It is illuminated by a spatial unit pulse and observed on the curved surface of a lens located at a normal distance $l = 2f$ of twice its focal length $f = 50\,\mathrm{mm}$ away. In the left half-image an additional diffraction pattern due to the discretization of the aperture is seen. It can be suppressed by introducing uniformly distributed jitter to the ξ/η grid coordinates, which yields the result in the right half-image. Note that the image makes use of a logarithmically scaled colormap representation to exhibit fine details.

aperture. The effect of a $5 \times 5\,\mu\mathrm{m}^2$ resolution of a $2.56 \times 2.56\,\mathrm{mm}^2$ rectangular aperture is shown in the left part of Fig. 5. To lessen the effect, which is not present in reality, an additional uniformly distributed jitter $\{d\xi, d\eta\}$ in the ξ- and η-coordinate is introduced, i. e. $\underline{E}(\xi_i, \eta_j)$ is replaced by $\underline{E}(\xi_i + d\xi_i, \eta_j + d\eta_j)$ with $|d\xi| < \Delta\xi/2$ and $|d\eta| < \Delta\eta/2$. This resembles a Monte-Carlo simulation of the input aperture, where the maximum distance between two samples is then given by $\sqrt{(4\,\Delta\xi^2 + 4\,\Delta\eta^2)}$ if two neighboring points get assigned maximum jitter values in opposite directions. The simulation result is shown in the right part of Fig. 5, where only the diffraction pattern of the aperture and not the one due to the source grid pixels is visible.

Unfortunately, the angles of vectors $\mathbf{r}_{ij}$ of points on the source grid to a single point on the screen get steeper with lesser observation distance. The phase differences between neighboring rays grow and thus errors are introduced, e. g. the field values at the perimeter of the lens should vanish in Fig. 5. A finer discretization of the source grid lowers the threshold distance for a valid simulation, but increases the complexity of the problem, i. e. the computation of diffrac-

tion patterns in the absolute near field requires an unreasonably fine spatial resolution. However, objective speckle patterns, simulated with this software framework, show a 'natural' behavior, i. e. the speckle size correlates negatively with surface roughness. The statistical process of speckle pattern generation is intact, albeit it uses far too less data to produce 'exact' speckles.

5. CONCLUSION

We showed that an artificial surface akin to a real, measured surface can be generated by means of a Fourier transform and that problems related to light propagation can be solved by means of GPGPU accelerated algorithms. The numerical approximation of the Huygens-Fresnel integral is well suited to simulate diffraction patterns in the optical far field. It performs good below the near/far field threshold of the Fraunhofer approximation, but poorly in the near field. Unfortunately, the simulation of reasonably sized lenses belongs to the latter regime. Despite these drawbacks objective speckle patterns are conditionally valid.

6. ACKNOWLEDGEMENT

We thank Mr. Lettner for some long and fruitful discussions and we also gratefully acknowledge the partial financial support for the work presented in this paper by the Austrian Research Promotion Agency and the Austrian COMET program supporting the Austrian Center of Competence in Mechatronics (ACCM).

7. REFERENCES

[1] D. Lee, J. Pelz, and B. Bhushan, "Scanning capacitance microscopy for thin film measurements," *Nanotechnology*, vol. 17, no. 5, p. 1484, 2006.

[2] D. Greszik, H. Yang, T. Dreier, and C. Schulz, "Measurement of water film thickness by laser-induced fluorescence and raman imaging," *Applied Physics B: Lasers and Optics*, vol. 102, pp. 123–132, 2011.

[3] F. Maier and B. Zagar, "Measurement of paint coating thickness by thermal transient method," *Instrumentation and Measurement, IEEE Transactions on*, vol. 58, no. 6, pp. 1958–1966, june 2009.

[4] R. S. Dwyer-Joyce, B. W. Drinkwater, and C. J. Donohoe, "The measurement of lubricant-film thickness using ultrasound," *Proc. R. Soc. Lond. A.*, vol. 459, no. 2032, pp. 957–976, 2003.

[5] D. Andelman, J.-F. Joanny, and M. Robbins, "Complete wetting on rough surfaces: Statics," *Europhysics Letters*, vol. 7, no. 8, pp. 731–736, Dec. 1988.

[6] R. R. Netz and D. Andelman, "Roughness-induced wetting," *Phys. Rev. E*, vol. 55, pp. 687–700, Jan 1997.

[7] J. Lettner and B. G. Zagar, "An application of laser speckle-based coating thickness measurement," *tm – Technisches Messen*, vol. 78, no. 11, p. 6, November 2011.

[8] D. Léger and J. C. Perrin, "Real-time measurement of surface roughness by correlation of speckle patterns," *J. Opt. Soc. Am.*, vol. 66, no. 11, pp. 1210–1217, Nov 1976.

[9] J. Dainty, *Laser Speckle and Related Phenomena.* Springer, 1984.

[10] J. W. Goodman, *Speckle Phenomena in Optics – Theory and Applications.* Roberts and Company Publishers, 2006.

[11] S. Equis and P. Jacquot, "Simulation of speckle complex amplitude: advocating the linear model," P. Slangen and C. Cerruti, Eds., vol. 6341, no. 1. SPIE, 2006, p. 634138.

[12] D. Goldberg, "What every computer scientist should know about floating-point arithmetic," *ACM Computing Surveys*, vol. 23, pp. 5–48, 1991.

[13] J. Bico, C. Tordeux, and D. Quéré, "Rough wetting," *Europhysics Letters*, vol. 55, no. 2, pp. 214–220, July 2001.

[14] D. Quéré, "Rough ideas on wetting," *Physica A: Statistical Mechanics and its Applications*, vol. 313, no. 1-2, pp. 32–46, 2002.

[15] R. C. Gonzales and R. E. Woods, *Digital Image Processing, 2nd Edition.* Prentice Hall, 2002.

[16] K. Creath and J. C. Wyant, "Absolute measurement of surface roughness," *Appl. Opt.*, vol. 29, no. 26, pp. 3823–3827, Sep 1990.

[17] G. Binnig, C. Quate, and C. Gerber, "Atomic force microscope," *Phys. Rev. Lett.*, vol. 56, pp. 930–933, Mar 1986.

[18] E. W. Otten, *Repetitorium Experimentalphysik*, 2003.

[19] J. W. Goodman, *Introduction to Fourier Optics – Second Edition.* The McGraw-Hill Companies, Inc., 1996.